Mediterranean Marine Science

Vol 3, No 2 (2002)

Development of a two-layer mathematical model for the study of hydrodynamic circulation in the sea. Application to the Thermaikos gulf

M.G. DODOU, Y.G. SAVVIDIS, Y.N. KRESTENITIS, C.G. KOUTITAS

doi: 10.12681/mms.245

Mediterranean Marine Science
Vol. 3/2, 2002, 05-25

Development of a two-layer mathematical model for the study of hydrodynamic circulation in the sea. Application to the Thermaikos gulf

M.G.DODOU, Y.G.SAVVIDIS, Y.N.KRESTENITIS and C.G.KOUTITAS

Division of Hydraulics & Environmental Engineering,
Dept. of Civil Eng. Aristotle University of Thessaloniki,
GR 54006 Thessaloniki, Greece

e-mail: mdodou@civil.auth.gr

Abstract

A two-layer hydrodynamic model for stratified flows has been developed and applied to the study of the sea water circulation in the Thermaikos Gulf (North Aegean Sea in the east Mediterranean Sea). The model was based on the finite differences method. The wind and Coriolis forces applied to a stratified basin (with initial density differences $\Delta\varrho/\varrho$ = 5‰) constituted the basic factors for the study of the circulation in the gulf, corresponding to the stratification conditions. The findings of the model, concerning the basic pattern of circulation in the gulf, were in accordance with in situ data collected in previous studies of the area. Furthermore, the application of the model allowed for the tracking and recognition of the regions of upwelling in the gulf, which were related to the prevailing wind conditions. For the integration of the research, the study was complemented with runs of a two dimensional – depth averaged- model which corresponded to non-stratified conditions. Comparisons and evaluation of the results of the simulations close the study.

Keywords: Mathematical models, Hydrodynamic circulation, Stratified flow, Upwelling, Wind curl.

Introduction

The hydrodynamic circulation of the seawater has been studied in detail during the last decades. The use of mathematical modeling contributed significantly to the progress of those studies and various mathematical models were developed in order to simulate the hydrodynamic circulation of the seawater masses due to different forcing factors.

CHRISTODOULOU *et al.* (1982), BLUMBERG *et al.* (1987), KOUTITAS (1987, 1988), KOURAFALOU *et al.* (1996, 1998), KRESTENITIS *et al.* (1997, 1998), SAVVIDIS *et al.* (2000), DODOU (2001) as well as many other researchers have successfully developed and applied mathematical models for the simulation of the coastal circulation. Those works included two-dimensional and three-dimensional mathematical models.

The selection and application of a two or three-dimensional mathematical model is based on the particular conditions of the vertical structure of the water mass and the level of the detail of the study pursued. Thus, the water

circulation of a non-stratified shallow coastal sea can be adequately described and studied by the application of a two-dimensional model. Wind driven flows or tidal circulations are often described by the application of two-dimensional models. On the other hand, if the vertical structure of the seawater masses is characterized by intense stratification, it is necessary to apply a three-dimensional mathematical model, so that the complicated physics of the flow can be described adequately.

The use of a two-layer mathematical model constitutes a significant alternative way of modeling the hydrodynamic circulation in the sea, because it combines the simplified mathematical approach and computer efficiency provided by the two-dimensional, depth-averaged models, with the advantages of the more detailed study of a multiple-layer stratified flow provided by the three-dimensional mathematical models.

Two-layered mathematical models are generally suitable for the simulation of stratified flows with a characteristic pycnocline, while an interesting application of those models is the simulation of upwelling and down welling events. Upwelling is the upward movement of the water from the deeper layers of the sea to the surface and constitutes one of the most important processes in the coastal ocean. More specifically, upwelling dynamics is considered to be a vital phenomenon for the fishery and life in the sea in general because it is related to nutrient regeneration in the surface layer.

Hydrodynamic circulation during the summer period in the Thermaikos Gulf (N. Greece) constitutes a representative example of wind-generated, vertically stratified flow. Due to a systematic decrease of the river flow input along the west coast of the Gulf, observed in recent decades, horizontal density differences are not included among the driving factors in our simulations. The main objective of this work was the development and application of a mathematical model of a two-layered flow which is proved to be a very practical tool for the simulation of Thermaikos Gulf water circulation under stratification conditions, including the special processes of upwelling events.

Delimination of the Gulf

The Thermaikos Gulf is located in the northern part of the Aegean Sea, situated north of the line of the Posidi- Platamonas capes, defining the eastern and western limits of that boundary. Figure 1.1 illustrates the gulf and its sub-regions according to Panayiotidis (PANAYOTIDIS, 1997): a) the Bay of Thessaloniki, occupying the northern part of the Thermaikos Gulf, and extending southwards to the line of Cape Micro Emvolo – Galikos river mouth, b) the Gulf of Thessaloniki, which extends from the line of Cape Micro Emvolo – Galikos river mouth, to the line of Cape Epanomi – Cape Atherida and c) the outer Thermaikos Gulf extending south from the Thessaloniki Gulf reaching the southern boundary line of Cape Posidi – Cape Platamonas.

As far as the accurate geographical position of the study area is concerned, it extends for about 80 km north of 39 .6° N and for about 75 km east of 22.6° E (KOURAFALOU *et al.*, 1998). The basin we studied extends from the shallow nearshore coastal areas (depths about 3 to 4 m) to the deep offshore sea with depths reaching to 100 m (Fig. 1.2).

Axios, Loudias and Aliakmon (and Pinios to the south, but just outside the computational domain) are the main rivers, outflowing along the west coasts of the Thermaikos Gulf.

Materials and Methods

Description of the two-dimensional, integrated in depth, mathematical model of coastal circulation

The general form of the mathematical model of coastal circulation constitutes a simplification of Reynolds equations based on the realistic assumption that the circulation of the water in the coastal field is nearly

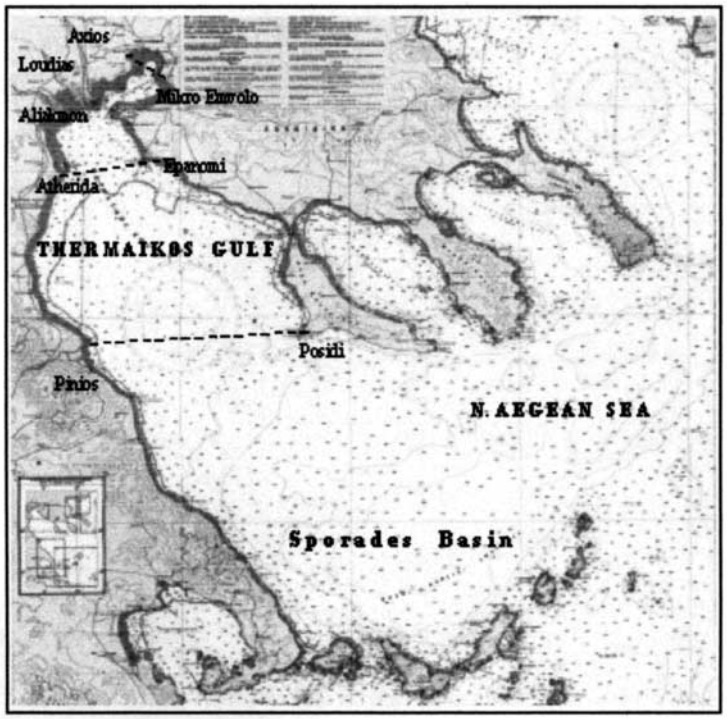

Fig. 1.1: Delimination of Thermaikos Gulf, distinction of the area in sub-zones and indication of the main outflowing rivers.

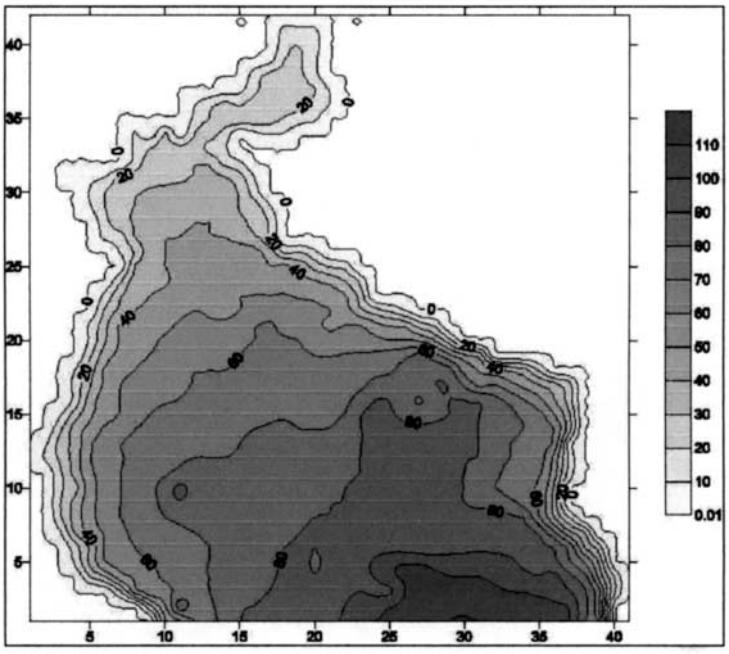

Fig. 1.2: Bathymetry of Thermaikos Gulf (depths contours in meters and axes in nautical miles).

horizontal, given that the horizontal dimensions of the coastal circulation field exceed considerably, in terms of magnitude, the vertical dimension of the water's depth (KOUTITAS, 1988). The assumption of nearly horizontal flow implies not only: a) the consideration of neglected vertical velocity components, but also b) a hydrostatic pressure distribution in depth with the respective expression of the horizontal pressure gradients,

$$\frac{\partial p}{\partial x} = \bar{\varrho}\, g\, \frac{\partial \zeta}{\partial x}\ ,\ \ \frac{\partial p}{\partial y} = \bar{\varrho}\, g\, \frac{\partial \zeta}{\partial y} \qquad (2.1)$$

where $\bar{\varrho}$ is the mean seawater density, g the gravity acceleration, ζ the elevation of the mean surface level from the stagnant level, c) the importance of the Coriolis forces influence (with their horizontal components) on a slowly developing flow,

$$f_{xc} = 2\Omega\, v \sin\varphi,\ \ f_{yc} = -2\Omega\, u \sin\varphi \qquad (2.2)$$

where $\Omega = 0.7297 \times 10^{-6}$ rad/sec the angular velocity of the earth's rotation, φ the latitude, and d) the turbulent character of the flow due to large Reynolds numbers, providing the application of the classical Boussinesq approximation for the description of Reynolds stresses,

$$\tau_{xz} = \varrho\, v_v\, \frac{\partial u}{\partial z}\ ,\ \ \tau_{yz} = \varrho\, v_v\, \frac{\partial v}{\partial z} \qquad (2.3)$$

where u, v are the velocity components along x and y axis respectively and v_v is the eddy viscosity coefficient in the vertical dimension. The model consists of the equations of mass and momentum conservation and the appropriate boundary conditions.

Momentum conservation equations

along x axis

$$\frac{\partial u}{\partial t} + u\frac{\partial u}{\partial t} + v\frac{\partial u}{\partial y} = -g\frac{\partial \zeta}{\partial x} + fv + \\ + \frac{\partial}{\partial x}\left(v_h \frac{\partial u}{\partial x}\right) + \frac{\partial}{\partial y}\left(v_h \frac{\partial u}{\partial y}\right) + \frac{\partial}{\partial z}\left(v_v \frac{\partial u}{\partial z}\right) \qquad (2.4)$$

along y axis

$$\frac{\partial v}{\partial t} + u\frac{\partial v}{\partial x} + v\frac{\partial v}{\partial y} = -g\frac{\partial \zeta}{\partial y} - fu + \\ + \frac{\partial}{\partial x}\left(v_h \frac{\partial v}{\partial x}\right) + \frac{\partial}{\partial y}\left(v_h \frac{\partial v}{\partial y}\right) + \frac{\partial}{\partial z}\left(v_v \frac{\partial v}{\partial z}\right) \qquad (2.5)$$

Mass conservation equation

$$\frac{\partial u}{\partial x} + \frac{\partial z}{\partial y} + \frac{\partial w}{\partial z} = 0 \qquad (2.6)$$

where u(x,y,z,t), v(x,y,z,t) and w(x,y,z,t) are the velocity components along x, y and z axis respectively, ζ(x,y,t) is the elevation of the mean surface level from the stagnant level and v_h, v_v are the eddy viscosity coefficients in the horizontal and vertical dimensions as functions of the hydrodynamic conditions.

Boundary conditions imply a) the equation of the Reynolds stresses on the free surface to the shear stress components τ_{sx}, τ_{sy} due to the wind velocity (free surface boundary condition),

$$\frac{\tau_{sx}}{\varrho} = KW_x\sqrt{W_x^2+W_y^2}\ ,\ \frac{\tau_{sy}}{\varrho} = KW_y\sqrt{W_x^2+W_y^2} \qquad (2.7)$$

where W_x, W_y are the wind velocity components at a distance of 10 m above the sea surface and K is a dimensionless constant with a magnitude of $1 \div 3 \times 10^{-6}$, b) the expression of shear stress components on the bed τ_{bx}, τ_{by} in terms of near bed velocities (bottom boundary condition),

$$\frac{\tau_{bx}}{\varrho} = C_f\, u\sqrt{u^2+v^2}\ \ ,\ \ \frac{\tau_{by}}{\varrho} = C_f\, v\sqrt{u^2+v^2} \qquad (2.8)$$

where C_f is a dimensionless constant with a magnitude ranging from 10^{-3} to 10^{-2} and c) the propagation of the radiated part of the surface elevation ζ_r from the inner basin to the open sea across the open sea boundary without back reflection (Sommerfeld radiation condition),

$$\frac{\partial \zeta_r}{\partial t} + C\frac{\partial \zeta_r}{\partial n} = 0 \qquad (2.9)$$

where n is the normal unit vector pointing outward the basin, C is the gravity waves propagation velocity.

The mathematical model described above can be further simplified if a logarithmic velocity distribution over the entire flow depth is assumed, in order to allow the expression of the equations (2.4), (2.5) and (2.6) in terms of the depth-averaged velocities, through integration along the flow depth h:

Momentum conservation equations

$$\frac{\partial U}{\partial t} + U\frac{\partial U}{\partial x} + v\frac{\partial U}{\partial y} =$$

$$= -g\frac{\partial \zeta}{\partial x} + \frac{\tau_{sx}}{\varrho h} - \frac{\tau_{bx}}{\varrho h} + fV + \nu_h \nabla_h^2 U \qquad (2.10)$$

$$\frac{\partial V}{\partial t} + U\frac{\partial V}{\partial x} + V\frac{\partial V}{\partial y} =$$

$$= -g\frac{\partial \zeta}{\partial y} + \frac{\tau_{sx}}{\varrho h} - \frac{\tau_{bx}}{\varrho h} - fU + \nu_h \nabla_h^2 V \qquad (2.11)$$

Mass conservation equation

$$\frac{\partial \zeta}{\partial t} + \frac{\partial}{\partial x}(Uh) + \frac{\partial}{\partial y}(Vh) = 0 \qquad (2.12)$$

Taking into account that real velocity profiles u, v in the case of wind-generated circulation deviate considerably from the logarithmic distribution, and in order to improve the non-linear acceleration terms approximation, the coefficients of the horizontal momentum diffusion ν_h are replaced with the horizontal momentum dispersion coefficients ν_h', where $\nu_h' > \nu_h$.

Description of the two-layer mathematical model of coastal circulation

In the case of vertical stratification of density, successive models of depth average flow are applied for each separate fluid layer. Provided measurements prove the existence of a pycnocline, the fluid can be treated as a two-layered one, by applying the equations of equilibrium and mass conservation for each layer separately. The unknown variables of the differential equations are the average depths h_o, h_u of upper and lower layer and the respective depth average velocity components U_o, V_o, U_u, V_u (Fig. 2.2).

An interesting point in a two-layered flow model is the development of shear stresses in the interface of the two layers related to the relative velocity of the two successive layers.

The model consists of the equations of mass and momentum conservation and the appropriate boundary conditions.

UPPER LAYER

Mass conservation equation

$$\frac{\partial h_o}{\partial t} + \frac{\partial}{\partial X}(U_o h_o) + \frac{\partial}{\partial Y}(V_o h_o) = 0 \qquad (2.13)$$

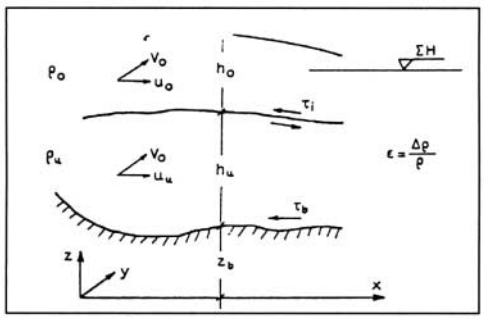

Fig. 2.2: A two layered stratified flow field structure with basic variable symbols, i.e. h_o, h_u for average depths of upper and lower layer, u_o, v_o, u_u, v_u for the respective depth average velocity components, ϱ_o, ϱ_u for average upper and lower layer densities, τ_b, τ_i for bottom and interface shear stress respectively, z_b bed distances from a reference axis (KOUTITAS *et al.,* 1994).

Momentum conservation equations along x-axis

$$\frac{\partial U_o}{\partial t} + U_o\frac{\partial U_o}{\partial x} + V_o\frac{\partial U_o}{\partial y} = $$
$$= -g\frac{\partial}{\partial x}\left(h_o + h_u + z_b\right) +$$
$$+ \frac{\tau_{sx}}{\varrho_o h_o} - \frac{\tau_{ix}}{\varrho_o h_o} + A_h \nabla_h^2 U_o + fV_o \qquad (2.14)$$

along y-axis

$$\frac{\partial V_o}{\partial t} + U_o\frac{\partial V_o}{\partial x} + V_o\frac{\partial V_o}{\partial y} = $$
$$= -g\frac{\partial}{\partial x}\left(h_o + h_u + z_b\right) +$$
$$+ \frac{\tau_{sy}}{\varrho_o h_o} - \frac{\tau_{iy}}{\varrho_o h_o} + A_h \nabla_h^2 V_o - fU_o \qquad (2.15)$$

LOWER LAYER
Mass conservation equation

$$\frac{\partial h_u}{\partial t} + \frac{\partial}{\partial x}\left(U_u h_u\right)\frac{\partial}{\partial y}\left(V_u h_u\right) = 0 \qquad (2.16)$$

Momentum conservation equations along x-axis

$$\frac{\partial U_u}{\partial t} + U_u\frac{\partial U_u}{\partial x} + V_u\frac{\partial U_u}{\partial y} = $$
$$= -g\frac{\partial}{\partial x}\left(h_u + z_b\right) - g\frac{\Delta\varrho}{\varrho}\frac{\partial h_o}{\partial x} +$$
$$+ \frac{\tau_{ix}}{\varrho_u h_u} - \frac{\tau_{bx}}{\varrho_u h_u} + A_h \nabla_h^2 U_u + fV_u \qquad (2.17)$$

along y-axis:

$$\frac{\partial V_u}{\partial t} + U_u\frac{\partial V_u}{\partial x} + V_u\frac{\partial V_u}{\partial y} = $$
$$= -g\frac{\partial}{\partial y}\left(h_o + h_u + z_b\right) - g\frac{\Delta\varrho}{\varrho}\frac{\partial h_o}{\partial y} +$$
$$+ \frac{\tau_{ix}}{\varrho_u h_u} - \frac{\tau_{by}}{\varrho_u h_u} + A_h \nabla_h^2 V_u - fU_u \qquad (2.18)$$

where ϱ_o and ϱ_u are the average upper and lower layer densities, $\frac{\Delta\varrho}{\varrho} = \frac{\varrho_u - \varrho_o}{\varrho_u}$ is the relative density, z_b is the bed distance from a reference axis and τ_{sx}, τ_{sy}, τ_{ix}, τ_{iy}, τ_{bx}, τ_{by} the surface, interface and bed shear stresses along x and y axes.

Boundary conditions refer to the surface, interface and bed, concerning the successive atmosphere influence on the upper layer, upper layer influence on the lower layer and bed influence on the lower layer.

Free surface boundary condition

$$\frac{\tau_{sx}}{\varrho_o} = k_s W_x\sqrt{W_x^2 + W_y^2}\ ,$$
$$\frac{\tau_{sy}}{\varrho_o} = k_s W_y\sqrt{W_x^2 + W_y^2} \qquad (2.19)$$

Boundary condition on the interface

$$\frac{\tau_{ix}}{\varrho_o} = \left(U_o - U_o\right)k_i\sqrt{\left(U_o - U_u\right)^2 + \left(V_o - V_o\right)^2},$$
$$\frac{\tau_{iy}}{\varrho_o} = \left(V_o - V_o\right)k_i\sqrt{\left(U_o - U_u\right)^2 + \left(V_o - V_u\right)^2} \qquad (2.20)$$

Bottom boundary condition

$$\frac{\tau_{bx}}{\varrho_o} = k_b U_u\sqrt{U_u^2 + V_u^2}\ ,$$
$$\frac{\tau_{by}}{\varrho_o} = k_b V_u\sqrt{U_u^2 + V_u^2} \qquad (2.21)$$

where k_s, k_i, k_b are the friction coefficients for the surface, interface and bed respectively with

$0[k_s] = 5.10^{-6}$, $0[k_i] = 10^{-3}$, $0[k_b] = 10^{-2}$, τ_{sx}, τ_{sy}, τ_{ix}, τ_{iy}, τ_{bx}, τ_{by} are the respective shear stresses and W_x, W_y are the wind velocity components. Boundary conditions are supplemented with the open sea boundary condition describing the free radiation of perturbation from the interior to the exterior infinite field:

Open sea boundary condition

$$\vec{V} \cdot \vec{n} \cdot h = \left(h - h_{initial} \right) \cdot C \qquad (2.22)$$

where n denotes the normal unit vector to the exterior of the field and C the gravity waves propagation velocity:

$$C_o = \sqrt{g\left(h_o + h_u\right)}$$

$$C_u = \sqrt{\frac{\Delta\varrho}{\varrho} g h_o \frac{h_u}{h_o + h_u}} \qquad (2.23)$$

Numerical solution of the mathematical models

For the numerical solution of both models a rectangular Arakawa C staggered grid was used where U, V components refer to the nodes sides, while ζ refers to the interior of each mesh (Fig. 2.1).

In the case of the first model the derivatives are approximated with explicit schemes of finite differences: time derivatives with forward differences and the other derivatives with central differences. In the case of the second model the numerical solution is based on a spatially centered scheme of second order explicit differences and a special 'leap frog' differences scheme for the approximation of temporal derivatives.

The stability of the numerical solution for both models is obtained through the satisfaction of relations between temporal discretization steps Δt and spatial discretization steps Δx or Δy, i.e. the CFL (Courant – Friedrichs – Lewy) criterion:

$$\Delta t < \frac{\Delta x}{\sqrt{2}\, C_{max}} \qquad (2.24)$$

where $C_{max} = \sqrt{g h_{max}}$ is the maximum phase velocity and h_{max} is the maximum depth observed.

Results

The two mathematical models, described above, have been applied to simulate the two different regimes of the water circulation in the Thermaikos Gulf observed during previous studies in the area.

The first regime considered was a nearly homogeneous water column in order to describe the case of a late autumn. During this period the plume of fresh water is usually small so that strong density gradients do not appear, neither does thermal stratification exist, as is obvious from a typical density profile (Fig. 3.1) measured in November '94 at the station TP22 (Fig. 3.2), in the framework of research

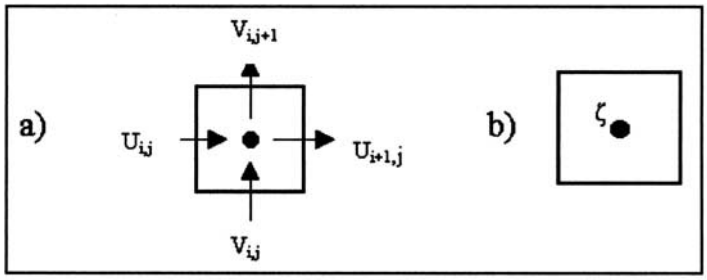

Fig. 2.1: The computational molecule for the horizontal and vertical velocity components U,V and the sea level ζ.

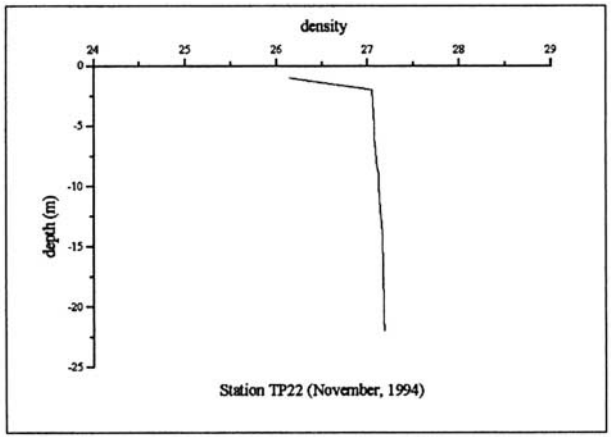

Fig. 3.1: Depth distribution of σ_θ density, measured at station TP22 in November 1994.

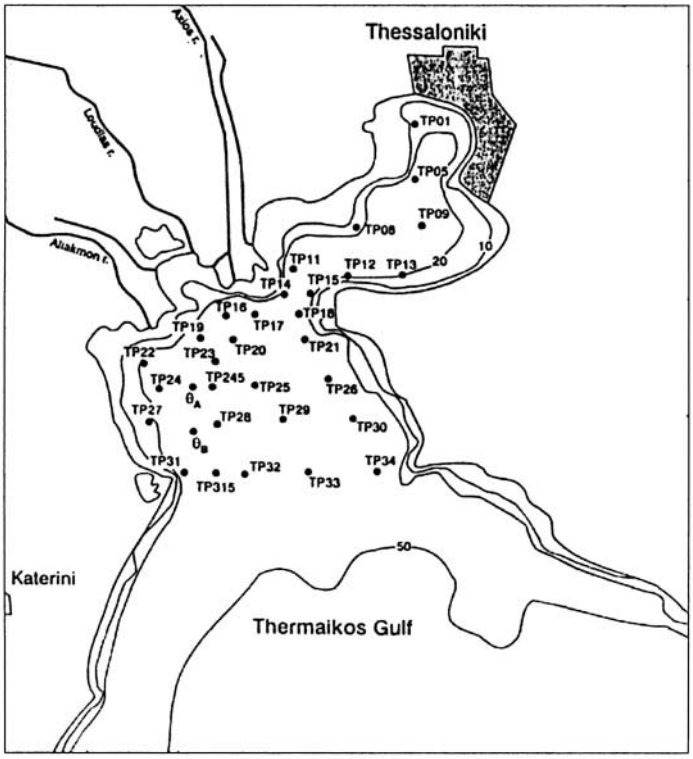

Fig. 3.2: A chart of the bathymetry over the survey area showing moorings ThA, ThB (marked θ_A, θ_B) and survey stations TP01-34 (KRESTENITIS *et al.,* 1997).

coordinated by Proudman Oceanographic Laboratory (P.O.L). In other words, the case of a barotropic, wind-generated circulation was examined, neglecting tidal currents through the cross section 'M.Emvolo – Axios Estuaries', since they are weak with an average tidal height of about 25 cm.

The second regime studied was a two-layer stratified basin approximating the summer case during which a surface mixed layer had formed

overlying a steep pycnocline, together with thermal and saline components. In particular, this is the case of July '94 (Fig. 3.3), when the plume expanded to the whole basin and there was a small halocline parallel to the deep thermocline.

This consideration is also suitable for the simulation of the case where the pycnocline coincides with the thermocline, which suggests that the plume of fresh water is small, resulting in haline homogeneity, as happened during August '94 (Fig. 3.4).

Measurements of the river discharges flowing into the Gulf have recently taken place and are summarized in Table 1 (KARAMANOS *et al.*, 1998), which implies that during summer the total discharges of the rivers are gradually minimized, giving the explanation of halocline suppression.

During the study of the summer baroclinic circulation, a surface layer of a 15-20 m thickness was adopted, as well as a steep pycnocline corresponding to a pycnometric difference of about 5‰, in order to be in agreement with density profiles in Figures 3.1, 3.3, 3.4, implying a temperature difference of more than 10°C between the two layers.

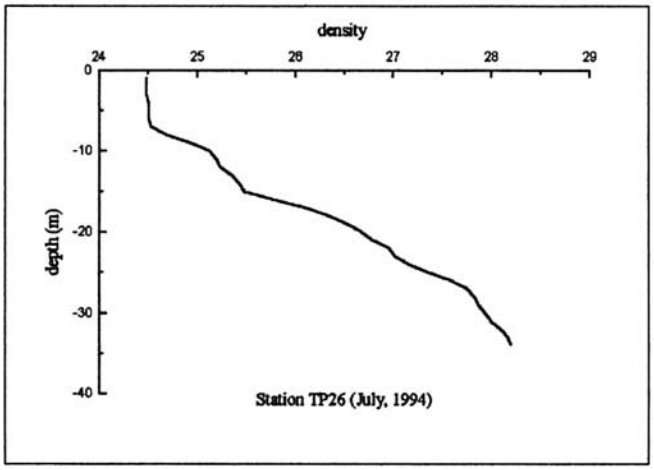

Fig. 3.3: Depth distribution of σ_θ density, measured at station TP22 in July 1994.

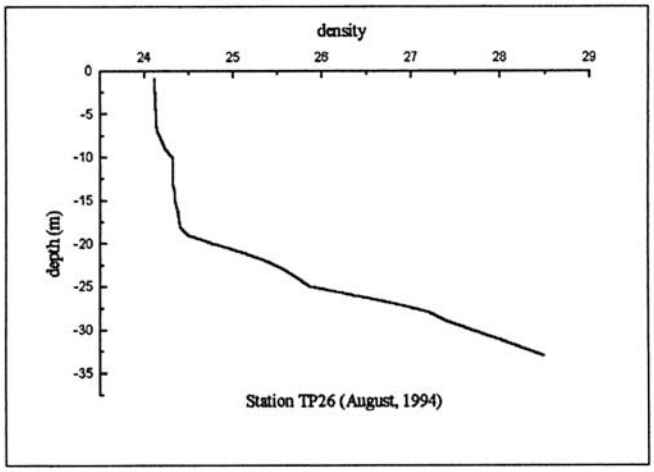

Fig. 3.4: Depth distribution of σ_θ density, measured at station TP22 in August 1994.

Table 1
Mean monthly water discharge of Axios, Loudias, Aliakmon for the period 1997-98 (KARAMANOS *et al.*, 1998).

RIVER WATER DISCHARGES (m^3/sec)			
Month	**Axios**	**Loudias**	**Aliakmonas**
January	174.21	34.87	79.15
February	149.73	13.77	96.60
March	155.39	11.71	32.00
April	97.00	40.00	11.23
May	85.08	34.76	37.15
June	**11.58**	**10.53**	**9.86**
July	**0.54**	**10.69**	**9.91**
August	**1.36**	**15.88**	**16.85**
September	37.55	22.78	33.36
October	108.44	16.62	24.84
November (*)	165.84	27.01	29.00
December	223.24	37.40	33.17
Total mean monthly water discharge ≈ 158.26 m^3/sec			

(*) interpolation between October and December

For both cases a constant wind velocity of 7 m/sec was applied. The wind direction was changed linearly along the y-axis from NNW at the northern boundary to NWW at the southern boundary of the basin, in order to approximate the curl of wind vectors such as the one shown in Figure 3.5, which constitutes the prevailing pattern of wind conditions.

The development of stratified flow has been further examined under the influence of constant NNW, NW and NWW winds, assuming a surface layer depth of 20 m in all cases, while the case considering variable wind direction was examined for two alternative surface layer depths:15 and 20 m respectively.

The computation grid was made by 41×42 grid points with a horizontal resolution of $\Delta x = \Delta y = 1852$m, it includes the Thermaikos Gulf as far as the cross section, 'Platamonas-Possidi'. A time step of 25 sec was used in order to satisfy the CFL criterion. The simulation was run until the establishment of a steady flow condition.

The model results are summarized in Table 2.

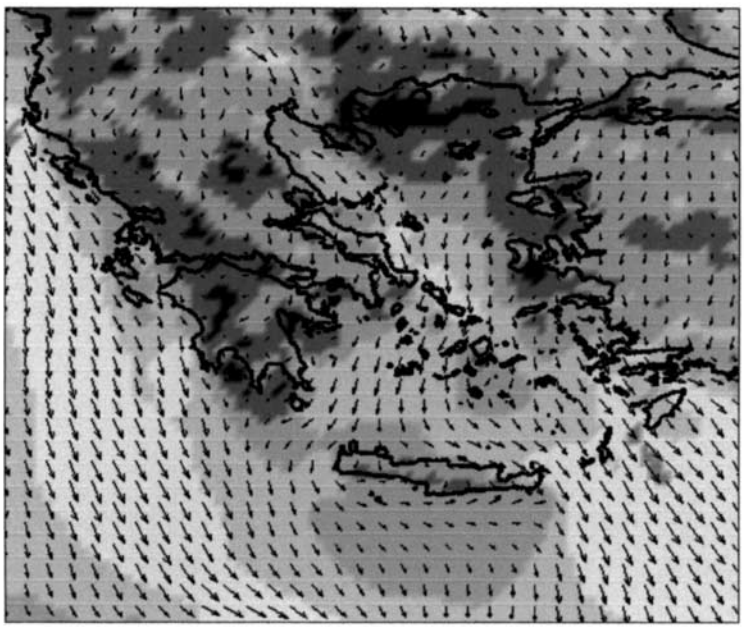

Fig. 3.5: Surface wind pattern forecast for 31.10.01 [POSEIDON System, http://www.poseidon.ncmr.gr].

Table 2
Summary of the different cases for which the two models were applied and the respective figures representing the results.

CASE A: Wind of 7 m/sec intensity and linearly variable direction from NNW at the northern boundary to NWW at the southern boundary of the field	
CASE A1: No stratified flow	Fig. 3.6
CASE A2: Stratified flow with a pycnocline at 20 m depth	Fig. 3.7a, 3.7b, 3.7c, 3.8d
CASE A3: Stratified flow with a pycnocline at 15 m depth	Fig. 3.8a, 3.8b
CASE B: Wind of 7 m/sec intensity and constant NNW direction Stratified flow with a pycnocline at 20 m depth	Fig. 3.9a, 3.9b
CASE C: Wind of 7 m/sec intensity and constant NW direction Stratified flow with a pycnocline at 20 m depth	Fig. 3.10a, 3.10b
CASE D: Wind of 7 m/sec intensity and constant NWW direction Stratified flow with a pycnocline at 20 m depth	Fig. 3.11a, 3.11b

Discussion

The application of both models using a realistic topography of the Thermaikos Gulf has raised the following interesting issues (DODOU, 2001):

- The circulation pattern is significantly influenced by the way that wind direction varies in the whole domain. The basic difference between the case of a variable wind direction (Figs 3.7c,b, 3.8c,d) and the three other cases with constant wind (Figs 3.9a,b, 3.10a,b, 3.11a,b) is focused on the circulation pattern of the upper layer, which tends to be anticyclonic for constant wind and cyclonic for variable wind, as far as wind direction is concerned (Ekman's spiral effect).
- An upwelling process takes place in some sub-regions of the coastal domain of the Thermaikos Gulf, depending on the prevailing wind conditions, as well as the density gradients. In the lower layer of the eastern part of the south open sea boundary, a characteristic inflow of seawater masses is observed, initially moving along the eastern coastline. As this movement takes place a section of the water masses moves to the (opposite) western side of the gulf. The remainder of the inflow masses continues its transport northerly -to the boundary of an upwelling region- where it turns again to the western coasts. Then, the currents follow the west coastline moving towards the western side of the south boundary and leave the gulf, continuing their transport to the open sea of the Sporades Basin (Figs 3.7d). A very important issue arising from the simulation is the observation that a section of the inflowing water masses enters the gulf from the eastern coasts and follows the basic trajectory of the north anticyclone. Then, these water masses come up to the surface of the upwelling region, refreshing the surface waters with cold, bottom waters, enriched with nutrients originating from the north Aegean Sea (and more specifically from the Black Sea). In this way, the results of the model simulations (concerning the hydrodynamic circulation in the gulf) are in line with the general circulation pattern presented by LYKOUSIS *et al.* (1981) (Fig. 4.1). This general pattern of water inflow and circulation in the Gulf constitutes a very strong point for the prognostic capability of the model.
- Another important point regarding the simulation, concerning the upwelling phenomenon, is related to the fact that the most favorable wind for upwelling events, in the case of shallow waters, is that normal to the coastline blowing toward the open sea, due to its collinearity with the Ekman's transport

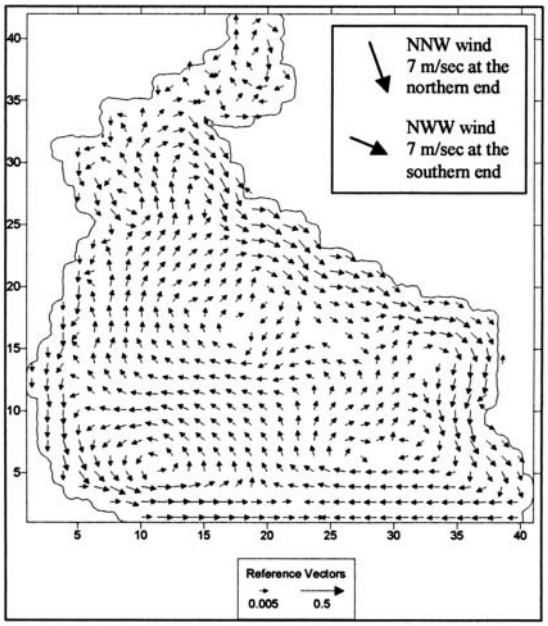

Fig. 3.6: Velocity pattern of non-stratified circulation under the influence of linearly variable wind from NNW at the northern boundary to NWW at the southern boundary (CASE A1). The axes are in nautical miles and the velocities in m/sec.

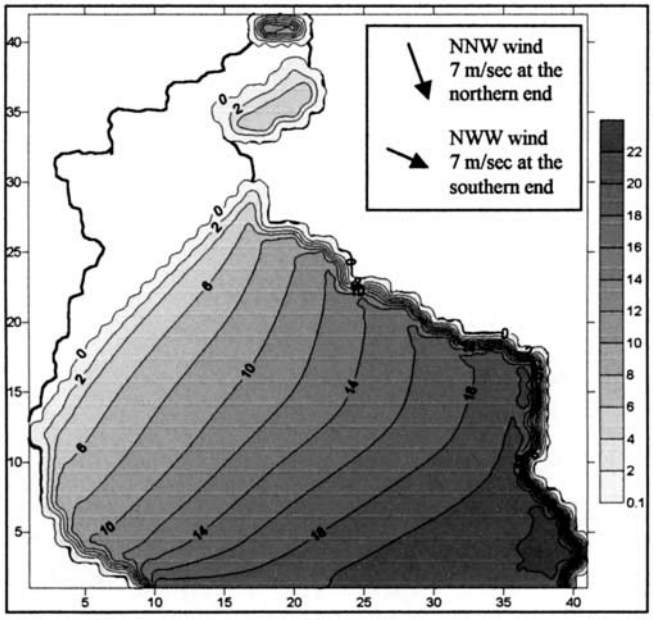

Fig. 3.7a: Contours of the upper layer thickness under the influence of linearly variable wind from NNW at the northern boundary to NWW at the southern boundary. The surface layer initial depth was 20m (CASE A2). The axes are in nautical miles and the thickness in meters.

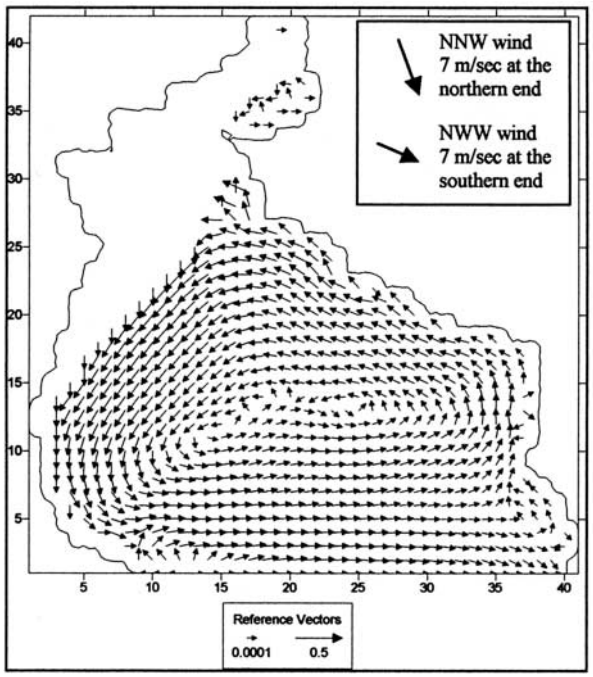

Fig. 3.7b: Contours of the lower layer thickness under the influence of linearly variable wind from NNW at the northern boundary to NWW at the southern boundary. The surface layer initial depth was 20m (CASE A2). The axes are in nautical miles and the thickness in meters.

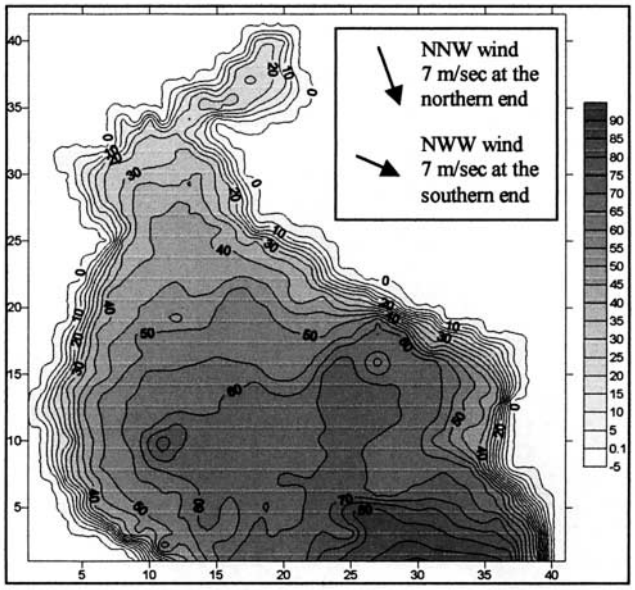

Fig. 3.7c: Velocity pattern of the upper layer under the influence of linearly variable wind from NNW at the northern boundary to NWW at the southern boundary. The surface layer initial depth was 20m (CASE A2). The axes are in nautical miles and the velocities in m/sec.

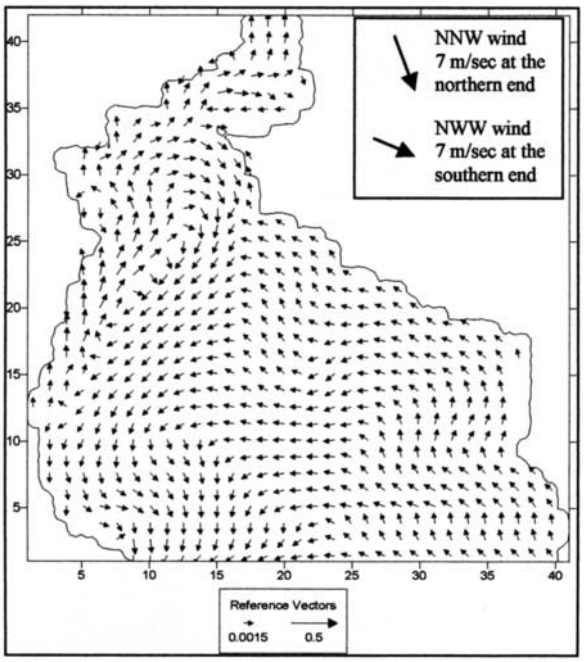

Fig. 3.7d: Velocity pattern of the lower layer under the influence of linearly variable wind from NNW at the northern boundary to NWW at the southern boundary. The surface layer initial depth was 20m (CASE A2). The axes are in nautical miles and the velocities in m/sec.

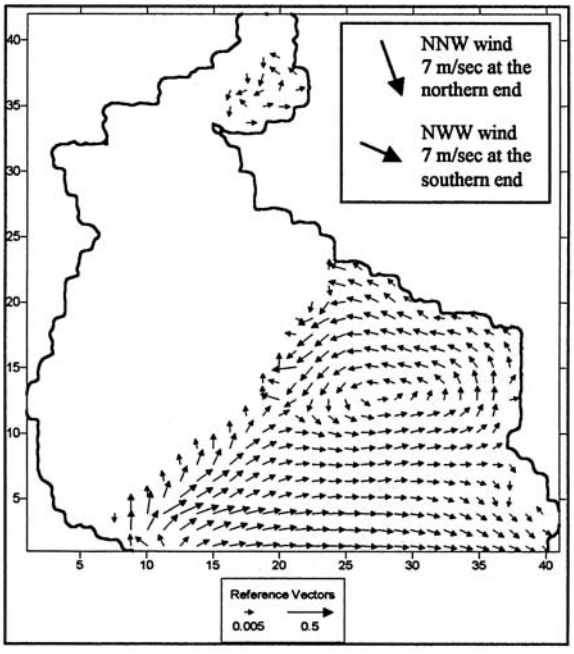

Fig. 3.8a: Velocity pattern of the upper layer under the influence of linearly variable wind from NNW at the northern boundary to NWW at the southern boundary. The surface layer initial depth was 15m (CASE A3). The axes are in nautical miles and the velocities in m/sec.

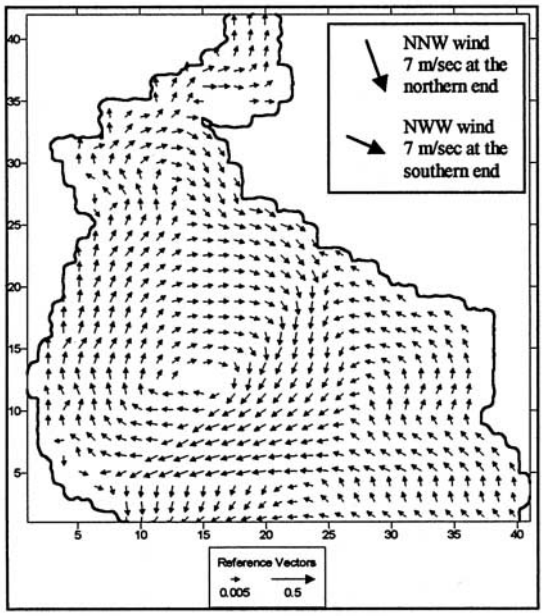

Fig. 3.8b: Velocity pattern of the lower layer under the influence of linearly variable wind from NNW at the northern boundary to NWW at the southern boundary. The surface layer initial depth was 15m (CASE A3). The axes are in nautical miles and the velocities in m/sec.

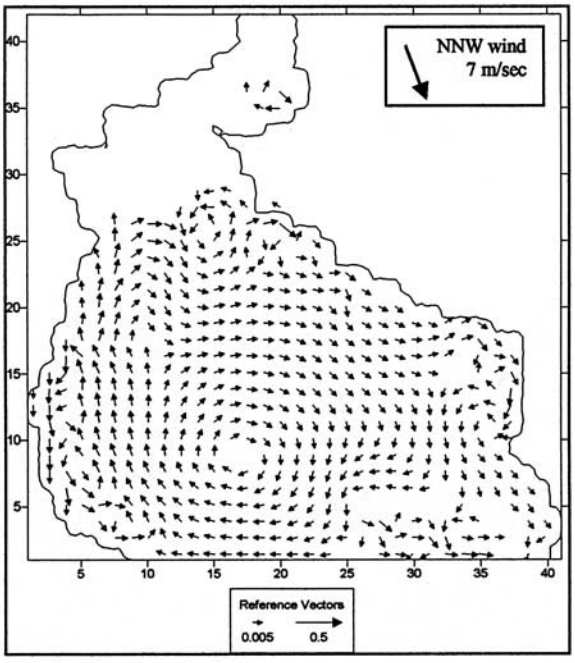

Fig. 3.9a: Velocity pattern of the upper layer under the influence of constant NNW wind. The surface layer initial depth was 20m (CASE B). The axes are in nautical miles and the velocities in m/sec.

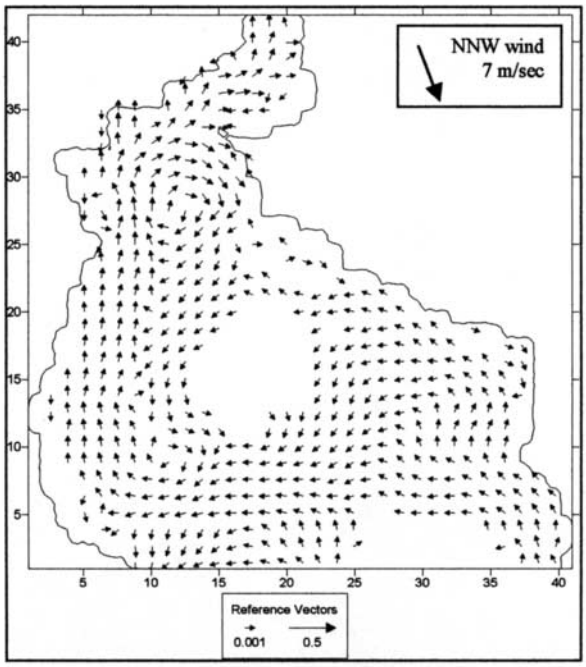

Fig. 3.9b: Velocity pattern of the lower layer under the influence of constant NNW wind. The surface layer initial depth was 20m (CASE B). The axes are in nautical miles and the velocities in m/sec.

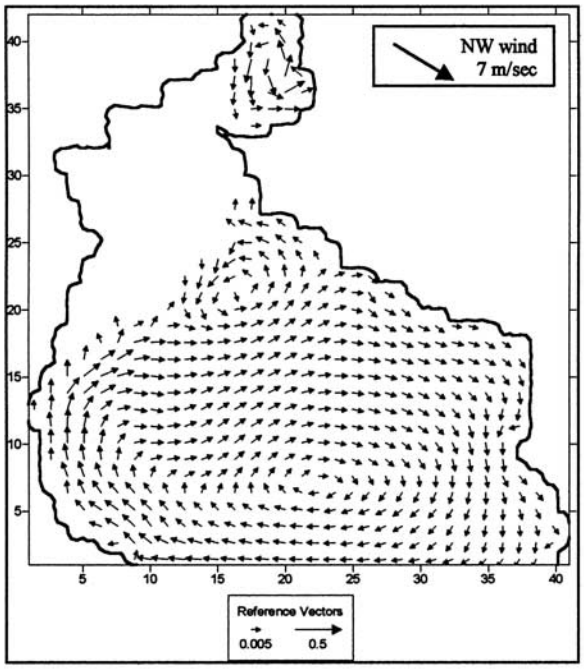

Fig. 3.10a: Velocity pattern of the upper layer under the influence of constant NW wind. The surface layer initial depth was 20m (CASE C). The axes are in nautical miles and the velocities in m/sec.

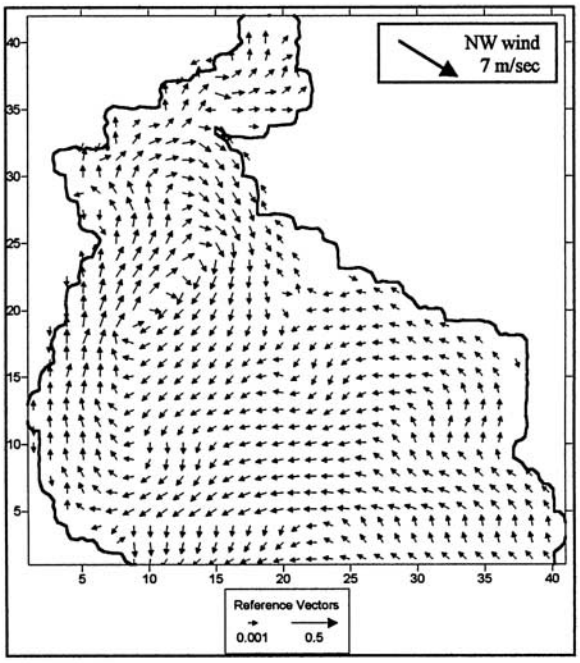

Fig. 3.10b: Velocity pattern of the lower layer under the influence of constant NW wind. The surface layer initial depth was 20m (CASE C).The axes are in nautical miles and the velocities in m/sec.

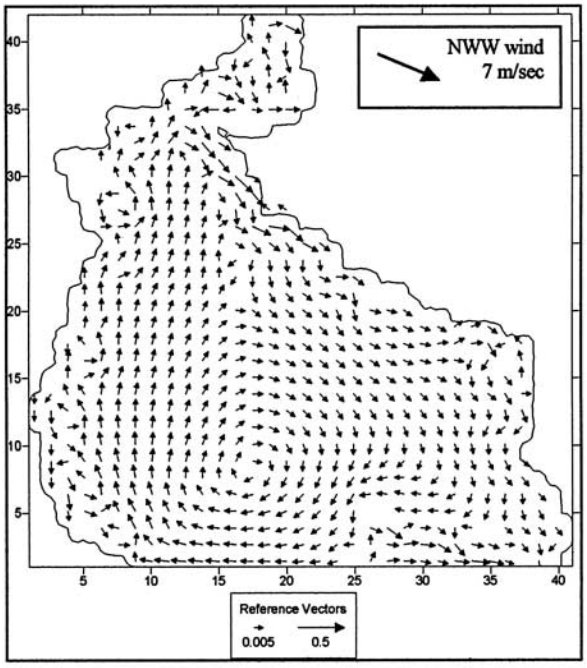

Fig. 3.11a: Velocity pattern of the upper layer under the influence of constant NWW wind. The surface layer initial depth was 20m (CASE D). The axes are in nautical miles and the velocities in m/sec.

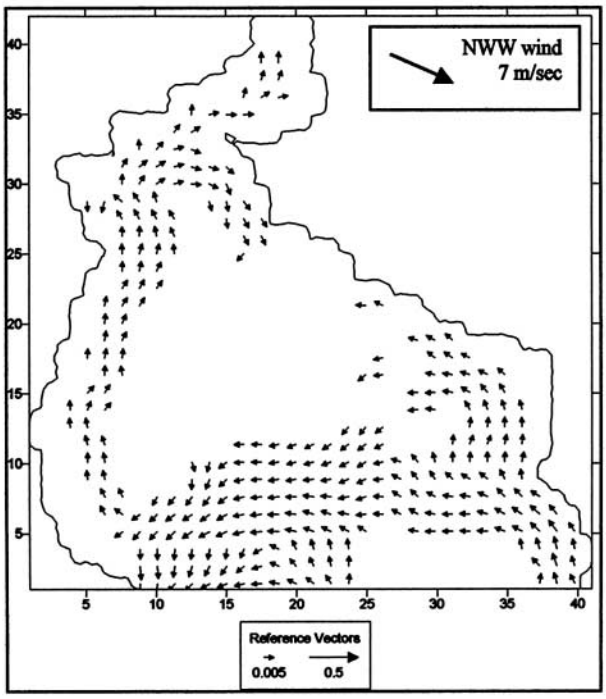

Fig. 3.11b: Velocity pattern of the lower layer under the influence of constant NWW wind. The surface layer initial depth was 20m (CASE D). The axes are in nautical miles and the velocities in m/sec.

Fig. 4.1: Schematic circulation pattern of Thermaikos Gulf proposed by LYKOUSIS e*t al.*, 1981.

direction. In this study, the prevailing NNW wind, along the northern coastal zones, is characterized by an important vertical component to the western part of the northern coastline, in this way generating significant transport of water mass towards the open sea. It is also remarkable that before the generation of the upwelling process, a current of 0,45 m/sec is strongly developed offshore of the western part of the north coastline. (Fig. 4.2).

The aforementioned observations support the theory of the zonation of the continental shelf, concerning the different process of upwelling dynamics (Fig. 4.3):

- Upwelling in the shallow coastal region (close to land) takes place when the wind blows towards the open sea (normal to the coastline).

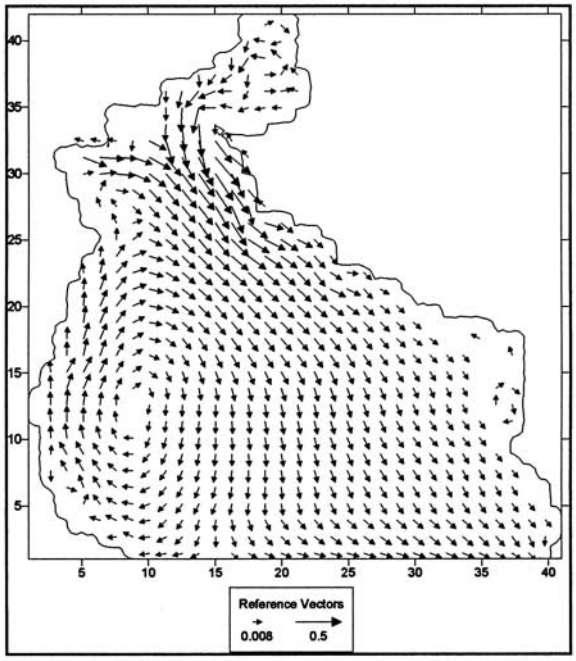

Fig. 4.2: Velocity pattern of the upper layer under the influence of linearly variable wind from NNW at the northern boundary to NWW at the southern boundary at time step 10 000 (2,7 hours). The surface layer initial depth was 20m.The axes are in nautical miles and the velocities in m/sec.

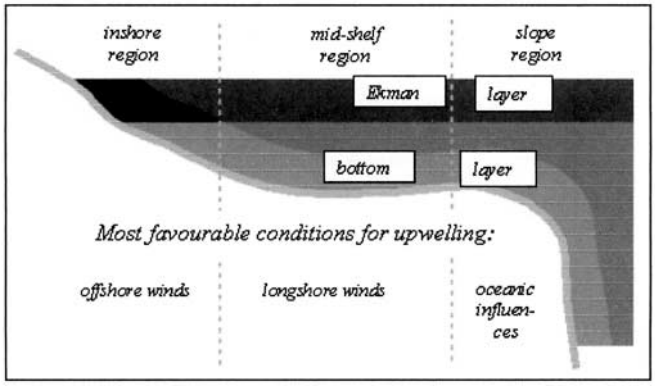

Fig. 4.3: Zonation of the coastal ocean into regions with different upwelling dynamics (TOMCZAK, 1996).

- Upwelling in the middle continental shelf develops under the influence of winds blowing parallel to the coastline, with the land to the left of their direction in the case of the northern hemisphere, or to the right in the case of south hemisphere.

- Furthermore, upwelling events can be observed in the external zone of the continental shelf, either due to ocean current variations or due to tidal pumping (TOMCZAK, 1996).

• Comparing the two cases for different thicknesses of the upper layer, 15 and 20 m, we can conclude that the water circulation of the upper layer as well as the lower layer presents the same features, and the main difference refers exclusively to the intense expansion of the upwelling region and the implicit decrease of the upper layer, which almost vanishes (Fig. 3.8a, b).

• The pattern of winter circulation (no stratified flow) which resulted from the application of a two - dimensional model is characterized by three anticyclones and a small cyclone (located at the south-eastern end of the model domain), suggesting that the wind curl influence is less determinant than the stratified flow case. (Fig. 3.6). An inefficiency of the model in describing water entrance into the gulf through the south -eastern open boundary is also observed.

• Summarizing the development and application of a two-layered hydrodynamic model presented in this paper helps to the better understanding of the physical mechanisms which govern the movements of the seawater masses in the case of stratified waters where a characteristic pycnocline has developed in the water column. In the case of the Thermaikos Gulf, the simulation of the wind vector field as a curl with important NW components, applied to a stratified, two-layered seawater flow, provides an adequate approximation of the gulf's prevailing circulation pattern and leads to a realistic description of the water refreshing mechanisms, i.e. the upwelling phenomenon.

References

BALOPOULOS, E., CHRONIS, G., LYKOUSIS, V. & PAPAGEORGIOU, E., 1987. Hydrodynamic and Sedimentological Processes in the North Aegean Sea: Thermaikos Plateau. Colloque International d' Oceanologie, ECOMEARGE, Perpignan, France.

BLUMBERG, A.F. &MELLOR G.L., 1987. A description of a three-dimensional coastal circulation model. p.1-16. In: *Three-dimensional Coastal Ocean Models*, edited by Norman S. Heaps, Washington, American Geophysical Union.

CHRISTODOULOU, G. & PROTOPAPAS, A., 1982. Water circulation and dispersion in the bay of Elefsina. *Technica Chronica*, 2, No. 1-2

DODOU, M., 2001. Mathematical models of stratified flows. Application for the study of circulation to Thermaikos Gulf during the summer period, M. Sc. Thesis, Thessaloniki, AUTh, 180p (in Greek).

KARAMANOS, H. & POLYZONIS, E., 1998. The adjacent land area and its potentiality for the fresh water and sediment supply. «Dynamics of Matter Transfer and Biogeochemical Cycles: Their Modeling in Coastal Systems of the Mediterranean Sea». A MAST-III ELOISE EU Project, Second Annual Scientific Report, Volume II.

KOURAFALOU, V., 1996. The fate of river discharge on the continental shelf 1. Modeling the river plume and the inner shelf coastal current. In: *Journal of Geophysical Research*, 101, No.C2: 3415-3434.

KOURAFALOU, V., KRESTENITIS, Y. & BARBOPOULOS, K., 1998. Modelling the seasonal variability of the processes that affect matter transfer on the Thermaikos Gulf. Part 1: land-sea interaction. «Dynamics of Matter Transfer and Biogeochemical Cycles: Their Modelling in Coastal Systems of the Mediterranean Sea». A MAST-III ELOISE EU Project, Second Annual Scientific Report, Volume II.

KOUTITAS, C., 1987. Three-Dimensional Models of Coastal Circulation: An Engineering Viewpoint, p.107-123. In: *Three-dimensional Coastal Ocean Models*, edited by Norman S. Heaps, Washington, American Geophysical Union.

KOUTITAS, C., 1988. Mathematical models in Coastal Engineering. London, Pentech Press Limited

KOUTITAS, C., HASILTZOGLOU, N., TRIANTAFILOU, G, KRESTENITIS, Y., 1994. Development and application of an operational mathematical model of density currents. Reprint of scientific yearbook in Polytechnic School, Department of Architecture, 1991-1993.

KRESTENITIS, Y.N., VALIOULIS I.A., CHRISTOPOULOS S.P., & HAYDER, P. A., 1997. The Rivers Influence on the Seasonal Coastal Circulation of the Thermaikos Gulf. In: *Proceedings of the Third International Conference on the Mediterranean Coastal Environment*, MEDCOAST 97, Malta.

LYKOUSIS., V., COLLINS, M.B., & FERENTINOS, G., 1981. Modern Sedimentation in the N. W. Aegean Sea. In: *Marine Geology*, 46: 111-130.

PANAYIOTIDIS, P., 1997. The role of the benthic primary production in the Land-Ocean Interaction Zone of the system Thermaikos Gulf- North Aegean Sea. «Dynamics of Matter Transfer and Biogeochemical Cycles: Their Modelling in Coastal Systems of the Mediterranean Sea», A MAST-III ELOISE EU Project, First Annual Scientific Report.

P.O.L. (Proudman Oceanographic Laborator), 1997. Processes in regions of freshwater influence – Profile. Final Report.

SAVVIDIS, Y. & KOUTITAS, C., 2000. Simulation of transport & fate of suspended matter along the coast of Agathoupolis (N. Greece). In: *Proceedings of the 5th International Conference Protection and Restoration of the Environment*, Thasos Greece.

TOMZACK, M., 1996, Shelf and Coastal Zone Lecture Notes, http://www.es.flinders.edu.au/~mattom/ShelfCoast/index.html.